Research Article

Exploring the Mechanism for the Photocatalytic Degradation of Oxytetracycline in Water using TiO_2 and Supplementary Oxidants

Tran Quoc Thao, Ngo Thi Thu Hien, Phan Thanh Lam and Nguyen Nhat Huy*
Faculty of Environment and Natural Resources, Ho Chi Minh City University of Technology (HCMUT), Ho Chi Minh City, Vietnam
Vietnam National University Ho Chi Minh City, Linh Trung Ward, Thu Duc City, Ho Chi Minh City, Vietnam

Pham Tan Thi
Faculty of Applied Science, Ho Chi Minh City University of Technology (HCMUT), Ho Chi Minh City, Vietnam
Vietnam National University Ho Chi Minh City, Linh Trung Ward, Thu Duc City, Ho Chi Minh City, Vietnam

Nguyen Trung Thanh, Phan Phuoc Toan and Le Tri Thich
Laboratory of Nanomaterial, An Giang University, Long Xuyen City, An Giang Province, Vietnam
Vietnam National University Ho Chi Minh City, Linh Trung Ward, Thu Duc City, Ho Chi Minh City, Vietnam

Nguyen Thi Thuy
School of Chemical and Environmental Engineering, International University, Ho Chi Minh City, Vietnam
Vietnam National University Ho Chi Minh City, Linh Trung Ward, Thu Duc City, Ho Chi Minh City, Vietnam

* Corresponding author. E-mail: nnhuy@hcmut.edu.vn DOI: 10.14416/j.asep.2024.11.007
Received: 22 August 2024; Revised: 4 October 2024; Accepted: 1 November 2024; Published online: 15 November 2024

Abstract
The persistent presence of antibiotics in wastewater, exemplified by oxytetracycline (OTC), poses environmental risks, necessitating robust removal strategies. This study investigates the effectiveness of photocatalysis utilizing TiO_2 (P25) treated at various temperatures, combined with different oxidants such as hydrogen peroxide (H_2O_2), potassium peroxydisulfate (PDS), potassium peroxomonosulfate (PMS) under diverse experimental conditions. The research systematically explores the impact of temperature, pH, and oxidant concentration on the efficiency of OTC degradation. Our findings reveal that the combination of P25/500, PDS, UV irradiation, and stirring demonstrates superior OTC degradation, surpassing 99% efficiency after 180 min. Optimal pH conditions are identified, emphasizing the importance of balancing acidity for enhanced performance. The study also provides insights into the optimal PDS concentration, indicating a threshold beyond which further increases yield diminishing returns. Mechanistic understanding is enhanced through scavenger experiments, elucidating the pivotal role of reactive oxygen species, particularly $O_2^{\bullet -}$, in the photocatalytic process. This research offers a practical framework for TiO_2-based photocatalysis in wastewater treatment, emphasizing tailored conditions for efficient antibiotic removal. The outcomes contribute valuable insights to the development of sustainable wastewater treatment protocols targeting antibiotic pollutants.

Keywords: Antibiotic degradation, Oxytetracycline, Photocatalysis, TiO_2 nanoparticles, Wastewater treatment

1 Introduction

The contemporary surge in antibiotic use raises concerns about their pervasive presence in the environment Huo *et al*., [1]. The global production and consumption of antibiotics have led to their widespread introduction into the environment through wastewater [2]. Antibiotic use in agriculture,

particularly in livestock and aquaculture, significantly contributes to environmental contamination, raising issues such as antibiotic resistance and inadequate wastewater treatment facilities [3]. The World Health Organization (WHO) underscores the urgency of reducing antibiotic use and developing efficient treatment strategies [4]. Over the past 50 years, antibiotics have played a pivotal role in inhibiting the growth or metabolic activity of microorganisms, leading to South Asian countries being at the forefront of antibiotic consumption [5], [6].

This paper examines the origins, challenges, and risks of environmental antibiotics, emphasizing β-lactam antibiotics, which constitute about 60% of global antibiotic use [2], and more persistent types such as tetracyclines, aminoglycosides, and macrolides. In Vietnam, pharmaceutical manufacturing leads to the discharge of antibiotic residues into water systems, posing environmental risks. Thai *et al*., [7] detected antibiotics like ampicillin, cefuroxime, and ciprofloxacin in wastewater, particularly from pharmaceutical plants, with sulfonamides and quinolones found at high concentrations, contributing to antibiotic resistance. While some antibiotics, such as β-lactams, degrade quickly, others like tetracyclines (e.g., oxytetracycline) persist in water and soil, exacerbating contamination. Though these residues can suppress harmful pathogens and enhance microbial biodegradation, they also act as selective pressures that encourage microbial communities to evolve and break down contaminants [8], [9]. However, these benefits are outweighed by the risks of resistance development, ecosystem disruption, and health threats through contaminated food and water.

OTC, a common tetracycline antibiotic, presents environmental challenges due to its in livestock and aquaculture [10]. Despite reports indicating that OTC concentrations in natural water bodies are as low as 2.1 ppb, laboratory studies often employ concentrations of 50–200 ppm to mimic real-world scenarios where adsorption or accumulation has occurred [11]. The widespread use of OTC is driven by its low cost and high effectiveness, but this leads to environmental contamination, as 30–90% of the administered antibiotic is excreted unchanged by animals [12]. In some regions, like Austria, surface water has been found to contain OTC levels as high as 46.91 ppm, while leachate samples in Shanghai have detected concentrations of 425.1 ppb. Furthermore, animal waste can carry up to 2.98 ppm of OTC, further contributing to pollution of both land and aquatic environments [11]. Understanding OTC degradation mechanisms is crucial for developing strategies to accelerate its environmental breakdown [13]. Antibiotics negatively impact wildlife, leading to bioaccumulation and long-term effects on various organisms [14]. Antibiotics in drinking water and food pose risks like antibiotic resistance, allergies, and toxicity.

Effective measures are essential for removing antibiotics from wastewater before they enter drainage systems [15]. Technologies such as electrolysis, membrane filtration, and advanced oxidation processes (AOPs) have been developed to address antibiotic pollution, but high costs and energy consumption limit their adoption [15]. Among the AOPs, photocatalysis using semiconductor materials, particularly TiO_2, is notable for effectively eliminating antibiotics in water [16]. TiO_2 photocatalysis is appealing due to its low cost, non-toxicity, chemical stability, and high electron exchangeability [17]. The photocatalytic mechanism of TiO_2 generates active radicals ($^{\bullet}OH$ and $^{\bullet}O_2^-$) that decompose organic pollutants [18]. Previous studies demonstrate the global application of TiO_2 photocatalysis in antibiotic degradation. In a case study in Vietnam, Tien *et al*., [19] reported 80% degradation of enrofloxacin using TiO_2 (P25) after 120 min under 40W mercury lamp irradiation. In other countries, Kakavandi *et. al*., [20] utilized modified TiO_2 for 93% degradation of tetracycline under UV/ultrasound irradiation. Similarly, Cai and Hu [21] reported 90% efficiency for sulfamethoxazole and trimethoprim using TiO_2 under UVA/LED light in 40 min. Additionally, TiO_2 synthesized via sol-gel methods has shown a 34.65% efficiency for Rhodamine-B degradation [22]. Bi-doped TiO_2 achieved 79.84% degradation of Rhodamine-B, while Ni-doped TiO_2 and Al/Ni-doped TiO_2 demonstrated 93% and high degradation efficiencies for Methylene Blue, respectively [23], [24]. Collectively, these studies underscore the versatility and effectiveness of TiO_2 in antibiotic degradation, reinforcing the potential of TiO_2 photocatalysis as a sustainable solution to environmental contamination by antibiotics.

This study provides a theoretical framework for assessing TiO_2 photocatalysis in treating OTC antibiotics, contributing to ongoing research on TiO_2 nanomaterials. The research outcomes offer insights into the reaction conditions and mechanisms that enhance TiO_2 photocatalytic capabilities, supporting future research and practical implementation.

Addressing antibiotic residues in wastewater is urgent, highlighting the potential application of photocatalysis in environmental remediation.

2 Materials and Methods

2.1 *Chemicals and experimental equipment*

OTC ($C_{22}H_{24}N_2O_9$) was procured from Kushan (China) as the target antibiotic. Commercial Degussa P25 TiO_2 nanopowder from Degussa AG (Germany) served as the photocatalyst. Key oxidizing agents included hydrogen peroxide (H_2O_2) from Duc Giang (Vietnam), potassium peroxydisulfate (PDS, $K_2S_2O_8$) from Xilong (China) and potassium peroxomonosulfate (PMS, oxone, $2KHSO_5.KHSO_4.K_2SO_4$) from Macklin (China). Sodium hydroxide (NaOH) and sulfuric acid (H_2SO_4) were obtained from Xilong (China). For radical scavenging tests, ammonium oxalate monohydrate ($(NH_4)_2C_2O_4.H_2O$, AO) was sourced from Shanghai Zhanyun (China), methanol (CH_3OH, MT) from Xilong (China), sodium azide (NaN_3, NN) from Himedia (India), and p-Benzoquinone ($C_6H_4O_2$, BQ) from Merck (Germany).

Photocatalytic activity was evaluated using a UV-visible spectrophotometer (DR6000, Hach, USA) to track OTC concentrations. Degradation efficiency was calculated as Equation (1):

$$\text{Degradation efficiency at t \%} = \frac{(C_i - C_t)}{C_i} \times 100 \quad (1)$$

Where C_i is the initial OTC concentration and C_t is the concentration at time t. FTIR identified functional groups involved in OTC degradation, and XRD analyzed changes in the TiO_2 crystalline structure before and after photocatalytic reactions [25].

Instrumentation utilized in the study included a 3W air pump, 25W magnet stirrer, and 8W UV lamps for analysis and photocatalytic processes. Morphological analysis of TiO_2 was conducted using scanning electron microscopy (SEM) equipped with energy-dispersive X-ray spectroscopy (EDX) on the JSM-IT200 equipment (JEOL, Japan). Chemical composition and functional groups present in the TiO_2 were analyzed using Fourier-transform infrared spectroscopy (FTIR) on the FT/IR-6X spectrometer (JASCO, Japan). X-ray diffraction (XRD) was performed using a D2 Phaser diffractometer (Bruker, Germany) to examine the crystalline structure of the materials. Optical properties were assessed using a spectrophotometer (U-3010, Hitachi, Japan). The identification of intermediates formed during OTC degradation was carried out using ultra-performance liquid chromatography-mass spectrometry (UPLC-MS/MS) on a Waters Xevo TDQ system (Waters, USA).

2.2 *Chemicals and experimental equipment*

OTC degradation experiments were conducted using a suspended photocatalytic model (Figure 1). Synthetic wastewater containing OTC and TiO_2 catalyst material was introduced into a reaction tank. The study involved the utilization of synthetic wastewater samples spiked with OTC antibiotic residues, which served as the primary subject of investigation. The synthetic wastewater was prepared in-house using distilled water and a known concentration of OTC to simulate real-world wastewater conditions. No human or animal subjects were involved in this research.

The reaction was initiated by aeration, mixing by magnetic stirrer, and the addition of oxidants (PDS, PMS, H_2O_2) under UV light exposure from an 8W black lamp positioned at the center of a reaction tank with a 100 mm diameter. Sampling at defined intervals (5 to 180 min) allowed for the assessment of treatment efficiency over time. Subsequent centrifugation and UV-Vis analysis were conducted to determine OTC.

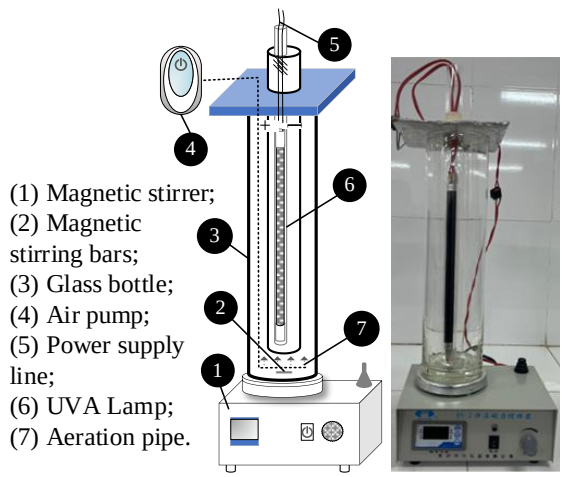

Figure 1: Experimental model for OTC photocatalytic degradation.

This study first investigates the photocatalytic degradation of OTC using P25 catalysts calcined at temperatures between 300 and 700 °C, testing their efficiency over various durations. The most efficient

catalyst was selected for further experiments (Section 3.2). Subsequent tests explored different TiO_2 photocatalyst and oxidant concentrations, and pH levels to determine optimal conditions for further experiments. The experiments were performed using catalyst concentrations between 100 and 500 ppm, with a fixed initial OTC concentration of 10 ppm, and PDS concentrations also ranging from 100 to 500 ppm. The pH values tested spanned from 3 to 11, with no adjustment made at the natural pH of 4.8. Experiments TN1 to TN30 examined OTC degradation with P25 under varying conditions, including UV light, different oxidants (H_2O_2, PDS, PMS), and stirring conditions. Finally, the study focused on detecting free radicals generated during photocatalysis and their effect on OTC treatment. Radical tests were performed using BQ for superoxide ($^{\bullet}O_2^-$), AO for photogenerated holes (h^+), NN for singlet oxygen ($^1O_2$), and MT for hydroxyl ($^{\bullet}OH$) radicals, all at a concentration of 5 mM.

3 Results and Discussion

3.1 *Properties of P25 nanomaterial*

In Figure 2, P25 calcinated at varying temperatures (300, 400, 500, 600, and 700 °C) was used for the photocatalytic degradation of OTC across different durations. The experiments were conducted with a fixed PDS concentration of 100 ppm, an unadjusted pH of 4.8, and an initial OTC concentration of 10 ppm. Among the samples, the result of the "P25/500" experiment was the most significant, demonstrating the highest efficiency, achieving 96.62% degradation after 180 min. Interestingly, the efficiency of P25/500 began to surpass the other samples around the 45 min mark, indicating its superior performance in accelerating the reaction rate early in the degradation process. Additionally, at 90 min, P25/500 exhibited a notable increase, clearly outpacing both P25/600 and P25/700. This suggests that the optimal calcination temperature of 500 °C provides a balance between structural and surface properties that maximize photocatalytic activity.

In contrast, the experiments with "P25/700" and "P25/600" showed peak efficiency occurred after 180 min as well, although their performances were slightly lower than that of P25/500. This highlights the significance of extended exposure to UV irradiation for the degradation of OTC, particularly for these higher-temperature calcinated samples.

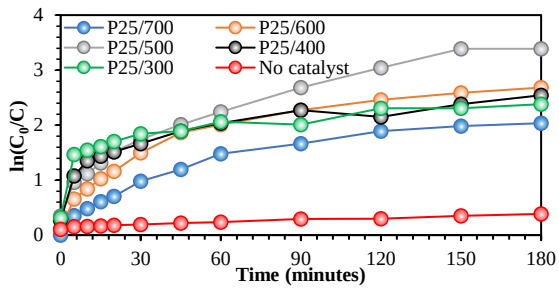

Figure 2: Effect of P25 treatment temperature on OTC photocatalytic degradation efficiency.

The lower temperature samples, "P25/400" and "P25/300," reached high efficiencies faster, around the 90-min mark, but showed signs of plateauing earlier than P25/500. This suggests quicker reactions but potential saturation points for these materials, where the prolonged exposure did not significantly improve their degradation performance. When compared to the "no catalyst" experiment, which only achieved 31.79% degradation after 180 min, it becomes evident that the photocatalyst plays a crucial role in enhancing the degradation of OTC. The "P25/500" catalyst, in particular, stands out for its superior degradation efficiency and was thus selected for further detailed analysis. Thus, the calcination temperature of 500 °C was selected for the subsequent control experiments as it demonstrated the highest efficiency in OTC degradation.

SEM and EDX were used to analyze the morphology and elemental composition of the synthesized TiO_2 catalyst (P25/500). SEM images revealed a structure more akin to pristine P25 rather than the anticipated tubular and porous TiO_2 morphology (Figures 3(a) and (b)). The SEM analysis reveals distinct differences in particle size and morphology between calcined TiO_2 (P25/500) and commercial P25. P25/500 exhibits larger, more irregular particles due to the calcination process, while pristine P25 maintains a finer, more uniform particle distribution characteristic of sol-gel synthesis. Both samples show agglomeration, which may affect their performance in photocatalytic applications. The structural similarity to the commercial form suggests that calcination at 500 °C enhances photocatalytic activity without significant morphological changes.

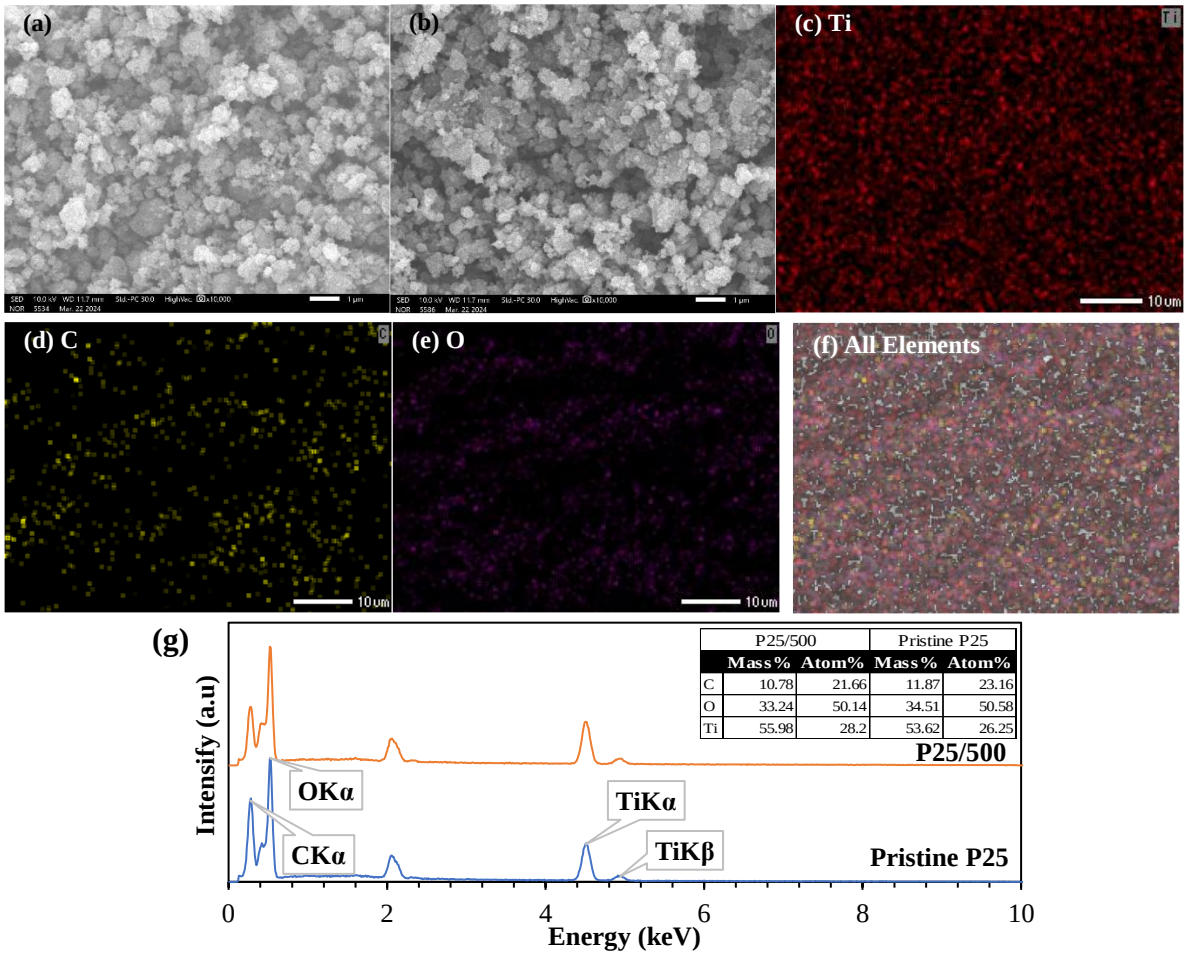

	P25/500		Pristine P25	
	Mass %	Atom%	Mass %	Atom%
C	10.78	21.66	11.87	23.16
O	33.24	50.14	34.51	50.58
Ti	55.98	28.2	53.62	26.25

Figure 3: SEM images of (a) commercial Degussa P25, (b) P25/500 (catalyst calcinated at 500 °C), (c) to (f) corresponding elemental mapping, (g) EDX of P25/500.

EDX and elemental mapping showed a uniform distribution of titanium (Ti) and oxygen (O), with minimal carbon (C) presence (Figures 3(c)–(g)). The presence of carbon may be attributed to surface contamination or sample preparation. However, this does not appear to impact the overall elemental distribution or the catalyst's performance, as the measured values for Ti and O align well with the expected stoichiometry of TiO_2. The EDX analysis of P25/500 exhibited peaks for Ti (Kα at 4.51 keV, Kβ at 4.91 keV), O (0.52 keV), and C (0.28 keV). Quantitative analysis indicated approximately 35.58% O, 16.94% C, and 47.48% Ti, aligning with the expected composition of TiO_2, confirming consistency with unmodified P25. Despite the lack of visible structural changes, P25/500 exhibits superior catalytic performance in degradation experiments, likely due to improved crystallinity or electronic properties from calcination. The consistent elemental composition further confirms the quality of the synthesized catalyst and underscores the minimal effect of surface impurities on its functionality.

The optical properties of the photocatalyst were examined using UV-Vis spectroscopy, revealing a band gap of approximately 3.3 eV for P25, consistent with literature values (3 to 3.2 eV) for commercial Degussa P25 (Figure 4(a)) [26], [27].

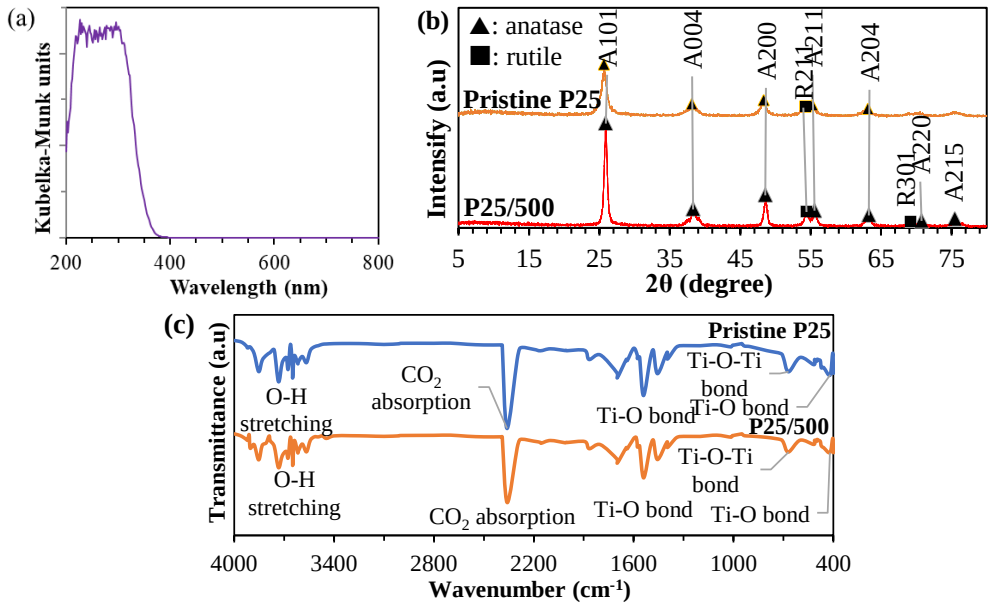

Figure 4: (a) UV–Vis absorption spectrum, (b) XRD, and (c) FTIR of P25/500.

XRD analysis with Cu-Kα X-rays (λ = 1.5406 Å) showed distinct peaks indicating the crystalline nature of TiO_2 nanoparticles. Both pristine and calcined P25 samples exhibited anatase and rutile phases with peaks consistent with known crystal indices [25]. Anatase peaks such as (101) at 25.9°, (004) at 38.3°, (200) at 48.6°, (211) at 55.6°, (213) at 63.3°, (220) at 70.8°, and (215) at 75.5°, along with rutile peaks (301) at 69.01° and (211) at 54.4° (according to PDF card No.021-1276 and 021-1272), are identifiable and consistent with the expected crystal indices [28]. Changes in peak positions or intensities between the pristine and calcined samples may indicate phase transformations or crystal growth (Figure 4(b)).

In Figure 4(c), FTIR spectra of pristine and calcined P25 revealed vibrational modes indicating TiO_2's chemical composition and structure [25]. Key peaks include Ti-O-Ti bonding at 669 cm^{-1} in the pristine sample, shifting to around 645 cm^{-1} post-calcination, indicating lattice alterations due to thermal stress. The presence of peaks around 1560–1600 cm^{-1} and 2300 cm^{-1} (CO_2 absorption) was noted. The absence of peaks at 1740 cm^{-1} suggests minimal carbonyl groups, indicating high TiO_2 purity. Broader wavenumber observations feature peaks around 3500 cm^{-1}, representing O-H stretching vibrations from surface hydroxyl groups [29].

3.2 *Study of the reaction mechanism of photocatalyst in OTC degradation*

3.2.1 Control experiments with OTC only

Control experiments without a catalyst were conducted with stirring (TN1) and UV irradiation with air exposure (TN2) (see Figure 5). The results show that UV irradiation and aeration are crucial for OTC degradation. UV light induces photolysis, breaking down OTC molecules, while aeration facilitates oxidative processes. The decrease in OTC concentration over time under TN2, where both UV irradiation and aeration are present, indicates active degradation mechanisms. In contrast, TN1, with only stirring and no UV irradiation, showed a slower degradation rate, highlighting the importance of UV light and aeration.

Compared to the study of Felis *et al*., [30], solar-driven processes achieved significant removal rates of trimethoprim and tetracycline to almost completely eliminated levels. According to Jin *et al*., [31], the direct photolysis of OTC, influenced by pH, concentration, and temperature, involves significant energy dissipation pathways and exhibits varying quantum yields among OTC species, setting the stage for comparison with the more robust and efficient photocatalysis process. These findings underscore the environmental significance of UV irradiation and

aeration in facilitating the natural degradation of antibiotics in aquatic environments, highlighting the potential for these processes to mitigate the presence of antibiotic residues and associated environmental risks.

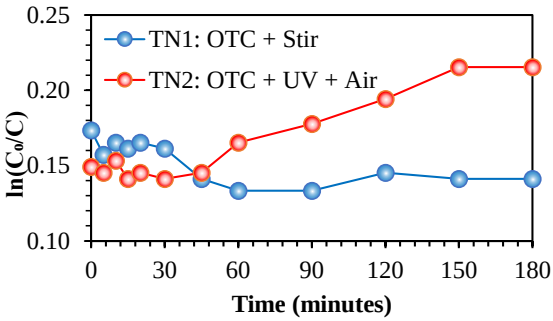

Figure 5: The photocatalytic degradation of OTC under catalyst-free conditions (TN1 and TN2).

3.2.2 Control experiments with catalyst only

In experiments, TN3 to TN6, the impact of P25/500, a commercial TiO_2, was evaluated under different conditions (see Figure 6). In TN3, only stirring without UV irradiation and aeration during photocatalytic degradation of OTC with P25/500 initially increased efficiency to 22% at 20 min but declined after 30 min, possibly due to site saturation or reactive species recombination. Conversely, TN4, with air exposure but no UV irradiation, saw a peak degradation efficiency of 40.41% at 180 min, indicating that prolonged air exposure is crucial for the degradation process.

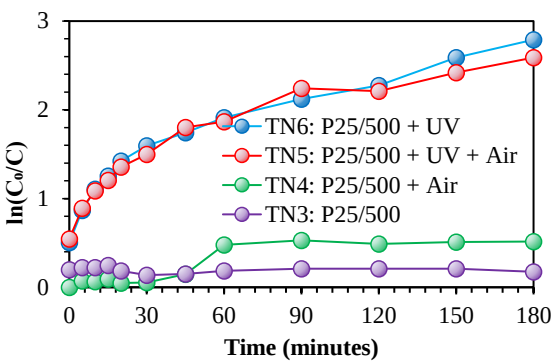

Figure 6: Impact of P25/500 catalyst on OTC degradation: UV, air, and stirring influences (TN3 to TN6).

Adding UV irradiation with air exposure (TN5) significantly improved degradation efficiency to 92.5% at 180 minutes, likely due to the generation of reactive oxygen species (ROS). Stirring with UV irradiation alone (TN6) also achieved a high efficiency of 93.86% at 180 minutes, confirming UV light as a key factor in OTC photocatalytic degradation.

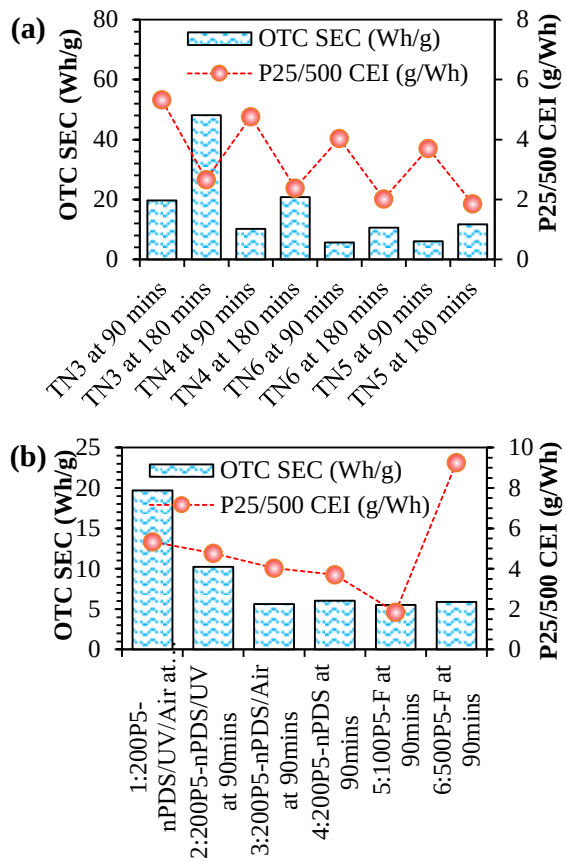

Figure 7: Energy consumption and degradation efficiency of (a) OTC degradation under UV, air, and stirring influences (TN3 to TN6) and (b) different P25/500 dosage. Note: 1:200P5-nPDS/UV/Air: 200ppm P25/500 without PDS, UV irradiation, and aeration; 2:200P5-nPDS/UV: 200ppm P25/500 without PDS and UV irradiation; 3:200P5-nPDS/Air: 200ppm P25/500 without PDS and aeration; 4:200P5-nPDS: 200ppm P25/500 without PDS; 5:100P5-F: 100ppm P25/500 with full operational conditions; and 6:500P5-F: 500ppm P25/500 with full operational conditions.

Figure 7 illustrates the comparison of energy consumption and degradation efficiency across various setups. In Figure 7(a), TN3, powered by a 25W magnetic stirrer, consumes 37.5 Wh in 90 minutes and 75 Wh in 180 min, demonstrating a higher specific energy consumption (SEC) for oxytetracycline (OTC) degradation, primarily due to the absence of UV irradiation and aeration. Although TN3 consumes moderate energy, its low degradation efficiency renders it less cost-effective compared to TN5 and TN6. TN4, utilizing a 3W air pump, is the most energy-efficient (4.5 Wh at 90 min), but its low degradation rate restricts its application in rapid treatments. TN5, combining an 8W UV lamp and a 3W air pump, optimizes energy consumption and efficiency (42 Wh in 180 min), while TN6, operating solely with UV light, achieves high degradation with lower energy use (24 Wh). In Figure 7(b), the comparison of different operational conditions (no PDS oxidant-"nPDS", UV irradiation-"UV", Aeration-"Air", and full operational condition-"F") and catalyst dosages (100 ppm-"100P" to 500 ppm-"500") reveals that the lowest dosage (100P) achieves the highest degradation efficiency (5:100P5-F at 90 minutes). Despite the lower energy intensity, the exclusion of PDS oxidant in this analysis is noteworthy, as adding PDS could raise costs and undermine the study's green chemistry focus.

3.2.3 Control experiments with oxidants only

In experiments TN19 to TN30, the focus was on exploring the photocatalytic degradation of OTC without the P25/500 catalyst (see Figure 8). These experiments examined various conditions: UV irradiation, stirring, and air exposure. TN19 to TN21 analyzed the effect of UV irradiation with air exposure (Figure 8(a)); TN22 to TN24 studied the influence of H_2O_2 (Figure 8(b)); TN25 to TN27 explored the impact of stirring (Figure 8(c)); and TN28 to TN30 combined H_2O_2 with stirring (Figure 8(d)). This investigation aimed to understand OTC degradation under diverse conditions without the P25/500 catalyst.

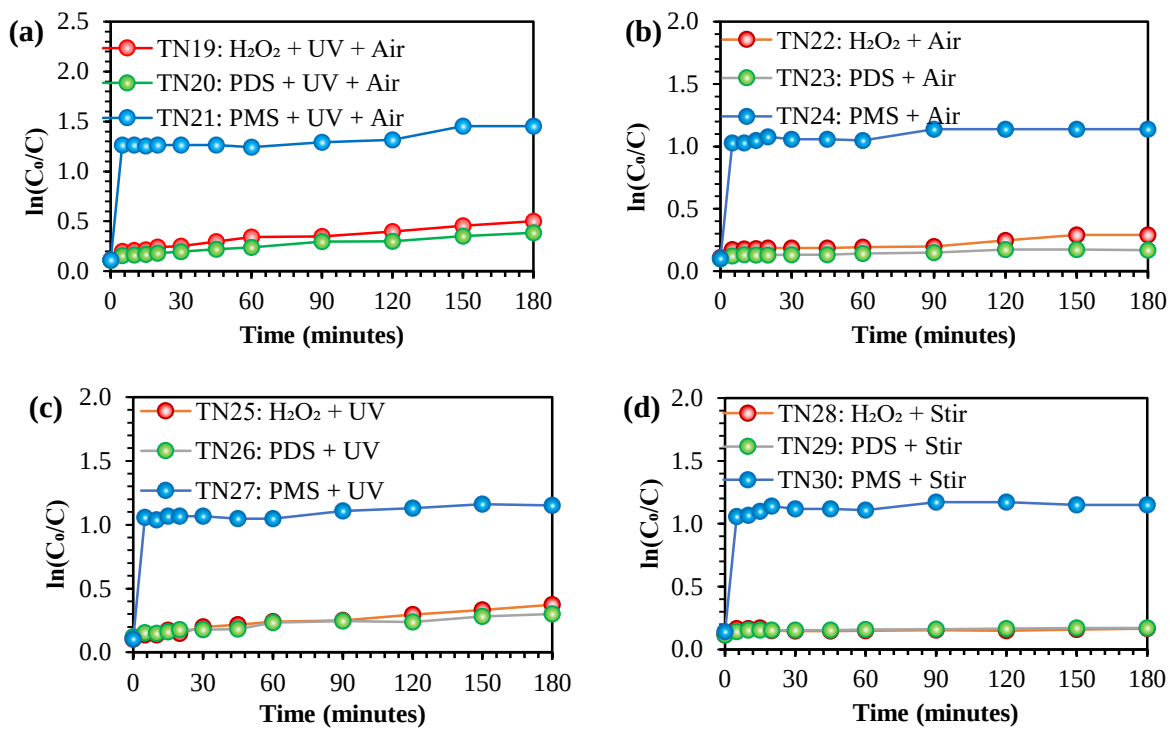

Figure 8: Comparative analysis of OTC photocatalysis with H_2O_2, PDS, and PMS under (a) UV and air (TN19 to TN21), (b) air (TN22 to TN24), (c) UV (TN25 to TN27), and (d) stirring influences (TN28 to TN30).

Experiments TN19 to TN21 analyzed the effect of UV irradiation with air exposure (Figure 8(a)). TN19, using H_2O_2 under UV and air, achieved approximately 39% efficiency. TN20, with UV and PDS, achieved around 32% efficiency, while TN21, with UV and PMS, showed about 77% efficiency. This highlights the significant role of UV light in enhancing the degradation efficiency. Experiments TN22 to TN24 studied the influence of H_2O_2 without UV (Figure 8(b)). TN22, without UV, had approximately 25% efficiency, underscoring the importance of UV light in the degradation process. TN23, with PDS and no UV, showed around 16% efficiency. TN24, with PMS and no UV, maintained about 68% efficiency, indicating that PMS is relatively effective even without UV. Experiments TN25 to TN27 explored the impact of stirring (Figure 8(c)). TN25, using H_2O_2 without stirring, achieved approximately 25% efficiency. TN26, with PDS and stirring, showed around 26% efficiency. TN27, with PMS and no stirring, achieved about 68% efficiency. These results suggest that stirring alone does not significantly enhance degradation efficiency compared to the use of PMS. Experiments TN28 to TN30 combined H_2O_2 with stirring (Figure 8(d)). TN28, using H_2O_2, achieved approximately 41% efficiency. TN29, with PDS, showed around 45% efficiency. TN30, using PMS, achieved the highest efficiency at about 72%. These results indicate the positive impact of stirring on OTC degradation.

Comparing TN19 to TN21 (air exposure) and TN25 to TN27 (no air exposure) offers insights into environmental conditions' impact on OTC degradation. TN19 to TN21, with air, showed H_2O_2, PDS, and PMS degradation efficiencies of 10.76%, 10.07%, and 10.76%. Without air, TN25 to TN27 showed higher efficiencies of 9.72%, 11.45%, and 10.07%. This suggests that the absence of air enhances OTC degradation. TN22 to TN30 results highlight different experimental conditions' impact on OTC degradation. TN22 to TN24, with air, had H_2O_2, PDS, and PMS efficiencies of 10.41%, 9.38%, and 9.72%. TN25 to TN27, under UV, showed H_2O_2, PDS, and PMS efficiencies of 9.72%, 11.45%, and 10.07%, demonstrating UV's pivotal role. TN28 to TN30, with stirring, had efficiencies of 10.76%, 10.76%, and 13.17%, indicating improved mass transfer and reaction kinetics.

PDS is chosen over PMS due to its superior performance in UV-assisted photodegradation, where the focus is on controlled radical generation. While PMS shows higher degradation efficiency without UV, it primarily follows an oxidation process, generating both sulfate and hydroxyl radicals. PDS, on the other hand, efficiently produces sulfate radicals under UV, ensuring sustained and selective photodegradation. This controlled reactivity under UV irradiation makes PDS a better fit for processes requiring precise management of the photocatalytic degradation pathway.

3.2.4 Experiments with photocatalyst (P25/500) under various conditions

The catalysts investigated include P25/500 combined with H_2O_2, PDS, and PMS, under UV irradiation and air exposure (see Figure 9). The following paragraphs present a comprehensive analysis of the results. The experimental groups (a) TN7 to TN9, (b) TN10 to TN12, (c) TN13 to TN15, and (d) TN16 to TN18 represent distinct conditions in the photocatalytic degradation of OTC employing P25/500 catalyst.

In Figure 9(a), the photocatalytic degradation efficiency improved over time, reaching 83.52% after 180 minutes (TN7). This indicates the synergistic effect of P25/500 and H_2O_2, combined with UV irradiation and air exposure, significantly enhances OTC degradation. The addition of H_2O_2 accelerates this process. PDS alongside P25/500 (TN8) showed a remarkable OTC degradation efficiency of 96.62%, and the combination of P25/500 and PMS under UV irradiation and air exposure (TN9) achieved 95.93%.

In Figure 9(b), TN10 (H_2O_2 and UV) showed consistent improvements in OTC degradation, reducing concentrations from 8.4 to 1.6 and achieving 83.52% removal efficiency. TN11 (PDS and UV) exhibited rapid degradation, stabilizing concentrations from 7.8 to 0.3, with 96.62% efficiency. TN12 (PMS and UV) reduced OTC concentrations from 8.3 to 0.4, resulting in 95.93% efficiency. Comparing TN7 to TN9 and TN10 to TN12 reveals that the absence of air enhances the efficiency of OTC degradation when using P25/500 with various catalytic agents.

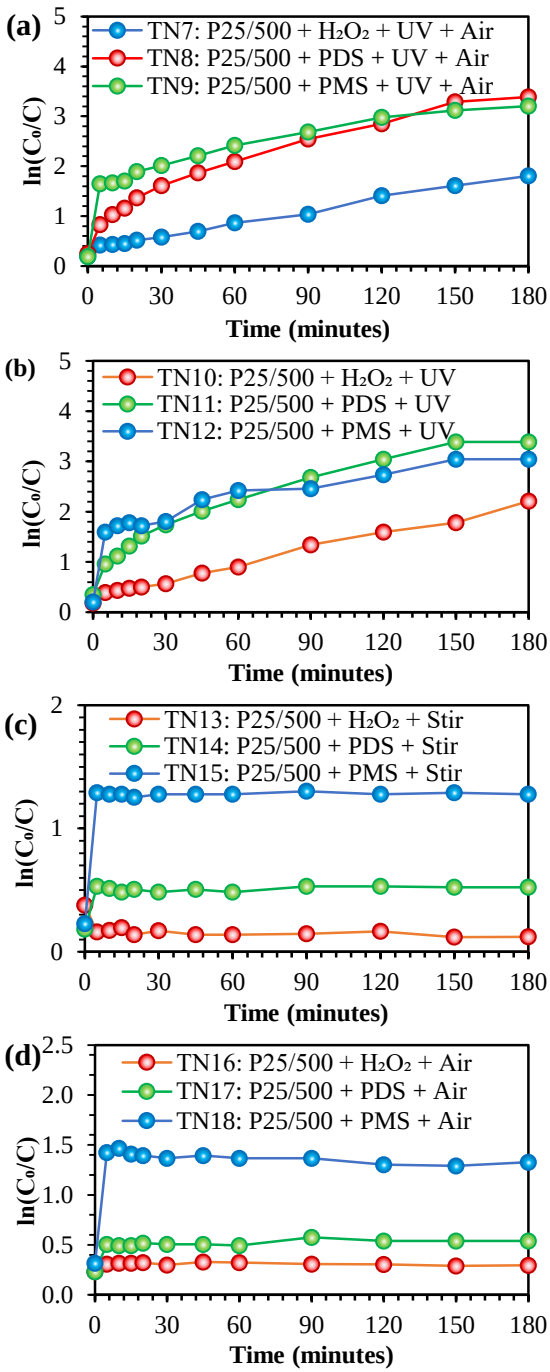

Figure 9: Comparative analysis of OTC photocatalysis: P25/500 with H_2O_2, PDS, and PMS under (a) UV and air (TN7 to TN9), (b) UV (TN10 to TN12), (c) stirring (TN13 to TN15), and (d) air influences

Stirring enhances mass transfer and promotes better contact between the catalyst and pollutant [32]. In TiO_2 photocatalytic processes, stirring improves mass transfer and catalyst dispersion, enhancing pollutant degradation. Aeration, by acting as an electron scavenger (providing oxygen), reduces charge recombination and boosts reaction rates, particularly for TiO_2, which benefits from additional oxygen as an electron acceptor [33]. However, excessive stirring can lessen the impact of aeration by reducing the effectiveness of air dissolution. Therefore, balancing stirring and aeration is key to optimizing photocatalytic performance [34]. In Figure 9(c), TN13 to TN15 involve P25/500 with H_2O_2, PDS, and PMS under stirring. TN13 (H_2O_2) reached 31.10% after 180 min, TN14 (PDS) achieved 40.76%, and TN15 (PMS) demonstrated an exceptional 95.24%, emphasizing the critical role of stirring in pollutant degradation.

In Figure 9(d), TN16 to TN18 analyzes the photocatalytic degradation of OTC using P25/500 with different oxidants (H_2O_2, PDS, PMS) under air exposure. TN16 (H_2O_2) showed steady efficiency, reaching 20.76% at 5 minutes. TN17 (PDS) and TN18 (PMS) followed similar trends, with TN18 peaking at 76.97%. Comparing TN7 to TN9 and TN16 to TN18 shows significant differences in OTC degradation under varying conditions. TN16 to TN18, without UV irradiation, demonstrated comparable or higher efficiencies than TN7 to TN9. This suggests that P25/500 with oxidants under air exposure can achieve significant OTC degradation, indicating potential for wastewater treatment applications.

3.2.5 Comparative analysis of catalytic degradation under various conditions

The data highlights the distinct roles of the oxidant alone (TN23, TN29), catalyst alone (TN14, TN17), and catalyst with oxidant (TN8, TN11) in the catalytic degradation process (see Figure 10).

In TN23 and TN29, where only the oxidant PDS is present, the $\ln(C_0/C)$ values remain relatively high, indicating the limited efficacy of PDS alone in catalyzing degradation. In TN17 (P25/500 with PDS under air) and TN14 (P25/500 with PDS under stirring), there is a moderate decrease in $\ln(C_0/C)$ values, suggesting that P25/500 alone has some catalytic ability, enhanced by stirring in TN14. TN8 (P25/500 + PDS + UV + Air) and TN11 (P25/500 + PDS + UV) show the most significant decrease in

ln(C_0/C), indicating that the combination of P25/500, PDS, and UV synergistically enhances degradation.

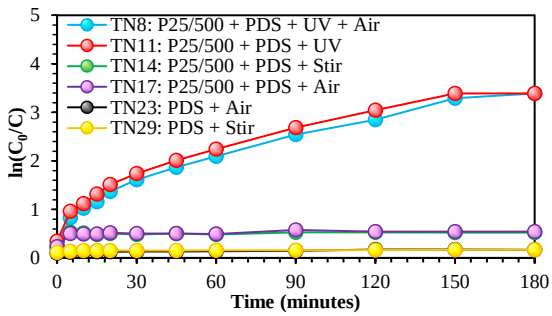

Figure 10: Comparative analysis of OTC photocatalytic degradation by different combinations of P25/500 catalyst and PDS under various conditions.

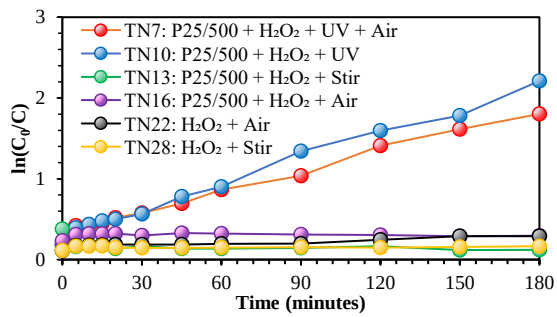

Figure 11: Comparative analysis of OTC photocatalytic degradation by different combinations of P25/500 catalyst and H_2O_2 under various conditions.

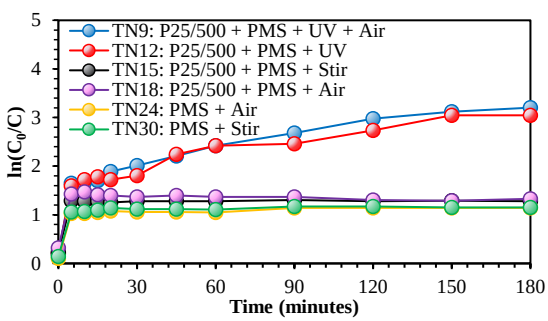

Figure 12: Comparative analysis of OTC photocatalytic degradation by different combinations of P25/500 catalyst and PMS under various conditions.

Figure 11 presents data on the degradation of a substance under various conditions involving different combinations of a P25/500, an oxidant (H_2O_2), and different environmental factors such as UV irradiation, stirring, and air exposure. The effectiveness of degradation varies significantly depending on the experimental conditions. The presence of TiO_2 enhances the degradation process, as seen by comparing TN22 and TN28 (oxidant alone) with TN16 and TN13 (catalyst and oxidant). UV irradiation further enhances degradation, as seen in TN10 compared to TN7. Stirring facilitates the degradation process, as evidenced by comparing TN16 and TN13. Air exposure does not significantly influence degradation under the given conditions, as seen by comparing TN14 and TN17.

Figure 12 shows the degradation of a substance under various experimental conditions with different combinations of catalysts, oxidants, UV irradiation, stirring, and air exposure. The catalyst used is P25/500, and the oxidant is potassium peroxydisulfate (PMS). The degradation efficiency varies over time with different conditions. PMS alone shows gradual degradation, while the combination of P25/500 and PMS enhances degradation efficiency. UV irradiation, stirring, and air exposure also influence the degradation process, with UV and stirring generally enhancing efficiency, while air exposure alone has a limited effect. Overall, the data highlights the complex interplay between catalyst, oxidant, and environmental factors in the degradation process, suggesting further analysis is necessary to optimize conditions for efficient degradation, potentially informing environmental remediation strategies.

3.3 *Evaluation of experimental conditions for control experiments*

3.3.1 Effect of pH value

Figure 13 shows the photocatalytic degradation efficiency (%) of oxytetracycline by P25/500 with PDS under different pH levels. Higher efficiencies are observed at values under pH 6 (including "No adjustment"), with optimal stability at pH 4.8. Efficiency increases with UV irradiation time, emphasizing UV light's crucial role. Stirring enhances degradation, especially at lower pH levels, while air exposure has a limited impact. At pH 3, efficiency improves from 20.41% at 5 min to 88.34% at 180 min, and at pH 4, it reaches 93.86% at 180 min, indicating a favorable slightly acidic to neutral range. Efficiencies at pH 5 and pH 6 peak at 86.97% and 86.28%, respectively, with a peak of 68.34% at pH 11. Remarkably, at no adjustment pH level of 4.8,

efficiencies remain consistently above 90%, leading to its selection for further subsequent experiments.

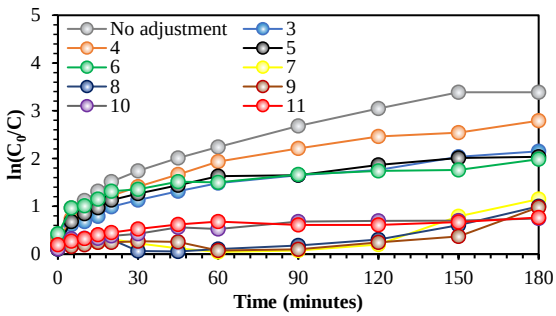

Figure 13: Photocatalytic degradation efficiency of OTC by P25/500 with PDS under various pH levels.

During the photocatalytic degradation of OTC in real wastewater starting at pH 5.2, a gradual drop in pH was observed. In the first 30 min, the pH decreased to around 4.9, likely due to the formation of acidic intermediates from OTC breakdown. By 120 min, the pH dropped further to 4.3, indicating continued production of acidic byproducts, such as carboxylic acids and CO_2. In the final phase (120–180 min), the pH stabilized around 4.4–4.5, suggesting a balance between the generation of acidic intermediates and their mineralization. This acidification is favorable for OTC degradation, as it enhances the interaction between the protonated TiO_2 surface and OTC molecules, improving photocatalytic efficiency. These results highlight the importance of pH stability in catalytic reactions and suggest that photocatalysis applications can align with green chemistry principles by operating effectively within a neutral pH range.

3.3.2 Effect of catalyst dosage

The investigation into the impact of oxidant PDS concentration, in conjunction with catalyst P25/500, on OTC photocatalytic degradation offers valuable insights into optimizing treatment conditions (see Figures 14 and 15).

Initially, at a fixed PDS concentration of 0.5g, increasing the P25/500 concentration from 100 to 500 ppm (with a ratio ranging from 1:1 to 1:5) led to a noticeable enhancement in photocatalytic degradation, achieving a peak OTC degradation efficiency of nearly 100% ($\ln(C_0/C) \approx 4.3$) after 180 minutes (Figure 14). This highlights the significant role of higher PDS concentrations in enhancing photocatalytic activity.

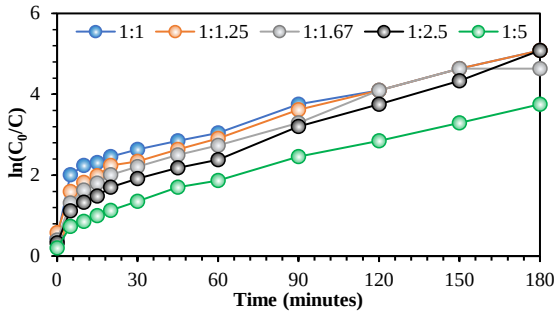

Figure 14: Comparative analysis of OTC photocatalysis degradation by different concentration ratios of P25/500 catalyst with PDS under UV influence.

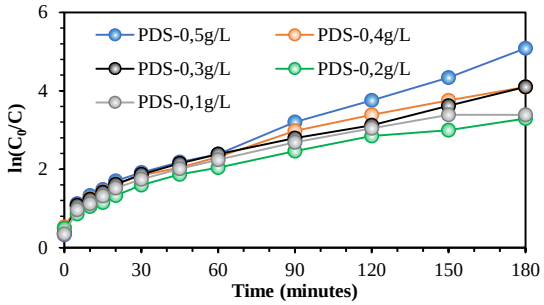

Figure 15: Comparative analysis of OTC photocatalysis degradation by P25/500 catalyst with different concentrations of PDS under UV influence.

However, as the PDS concentration decreases from 100 to 500 ppm while keeping P25/500 constant at 500 ppm, there is a gradual reduction in OTC degradation efficiency (Figure 15). Despite the decrement, a substantial removal efficiency of 96.62% ($\ln(C_0/C) \approx 3.4$) is maintained at the lowest PDS concentration. This indicates the robustness of the photocatalytic system, even under suboptimal PDS concentrations, potentially offering cost-effective alternatives for large-scale applications. Comparative analysis of lower PDS concentrations (200, 300, and 400 ppm) shows a proportional relationship between PDS concentration and OTC removal efficiency, peaking at 98.34% ($\ln(C_0/C) \approx 3.9$) at a 200 ppm concentration after 180 minutes. This suggests a threshold concentration beyond, which further increases may not significantly enhance degradation efficiency. The findings indicate that P25/500 at 500ppm provides the optimal balance for efficient OTC degradation under the experimental conditions. In comparison, Azadi *et al.*, [35], employing the response surface methodology for optimization,

achieved a maximum OTC degradation efficiency of 89.3% under the conditions of 0.28 g/L P25/Fe^0/ZnO at 3.02 mg/L of PDS and pH 7.5 after 120 min.

3.3.3 Effect of light source

The comparison between natural sunlight and UV-driven photocatalysis was evaluated under identical conditions (catalyst and PDS dosage, stirring, and aeration), as shown in Figure 16.

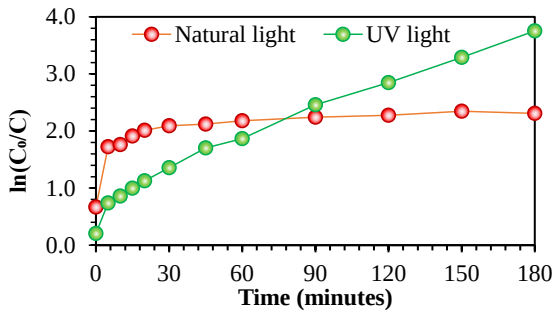

Figure 16: Comparison of OTC degradation efficiency over time between natural light-driven and UV-driven photocatalytic systems.

The UV-driven system demonstrated significantly faster degradation, with 97.66% efficiency at 180 minutes, compared to 90.07% under natural light. The higher initial degradation in the natural light-driven system (48.69%) compared to UV-driven (18.34%) is attributed to the adsorption process during the 30-min-period without irradiation. Both experiments were shielded from light, ensuring that no irradiation influenced the adsorption phase. However, slight variations in the catalyst's surface charge, ambient temperature, or mixing efficiency could have contributed to improved adsorption in the natural light-driven setup. After 60 min, the UV-driven setup outpaced the natural light system, reaching 84.55% degradation versus 88.69% for natural light. By contrast, Zhang *et. al.*, [36] reported a degradation efficiency of approximately 60% after 5 h under conditions of pH 5.7 with 10 ppm OTC and 500 ppm TiO_2. This trend continues, with UV-driven degradation efficiency reaching 96.28% by 150 min, compared to 90.41% for natural light. The UV-driven system's consistency and higher energy intensity led to superior performance in a controlled environment. However, natural sunlight remains an attractive option for large-scale applications due to lower operational costs, despite its lower and more variable efficiency. Practical implementation would require optimizing natural sunlight systems to maintain performance levels comparable to UV-driven systems.

3.4 *Practical application of P25/500 in real-world scenario*

An additional experiment was conducted using an actual water sample collected from a natural water body with an initial OTC concentration of 8.45 ppm, compared to the standard laboratory experiments under identical conditions (500 ppm P25 catalyst, 500 ppm peroxydisulfate (PDS), UV irradiation, stirring, and aeration) (see Figure 17). This experiment aimed to evaluate the performance of the photocatalytic system in a real-world scenario.

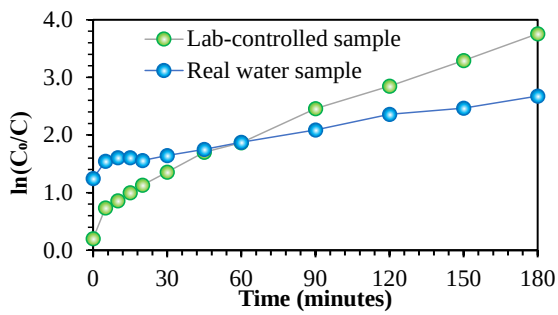

Figure 17: Comparative degradation efficiency of OTC in natural water sample versus synthetic solution.

The degradation efficiency in the actual water sample showed a notable decrease compared to synthetic OTC solutions. In the lab-controlled environment, OTC degradation reached over 90% at the 90-min mark, while the natural water sample achieved that degradation efficiency after 180 min. This decline can be attributed to several factors inherent to real-world water matrices, including the presence of organic matter, suspended solids, and inorganic ions (e.g., carbonate, chloride, nitrate) that may interfere with the photocatalytic process by scavenging reactive radicals or adsorbing onto the catalyst surface [37].

In practical applications, these findings suggest that while the P25/500 system performs well in controlled conditions, additional treatment steps may be required for natural water matrices to enhance its efficacy. Pre-treatment methods, such as filtration to remove suspended particles, or the addition of radical-enhancing agents, could potentially improve

degradation rates. Furthermore, the robustness of the system needs to be evaluated for varying environmental conditions, such as fluctuations in pH, ionic strength, and organic load, which are often observed in water bodies.

Recycling experiments were conducted to evaluate the potential degradation efficiency of P25/500 over time using an initial 10 ppm oxytetracycline (OTC) concentration, 300 ppm catalyst, and 500 ppm peroxydisulfate (PDS) across four 180-min cycles. The data presented in Figure 18 provides a detailed view of the system's performance across these cycles.

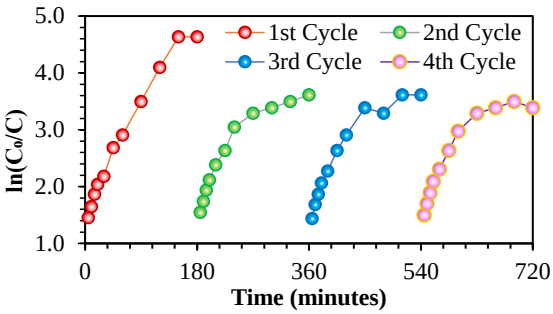

Figure 18: Degradation efficiency of OTC over four 180-min cycles using P25/500 catalyst.

In the first cycle, the degradation follows a typical logarithmic trend increasing steadily from the 5-min mark to the 180-min mark, demonstrating the strong oxidative capacity of the P25/500 catalyst and PDS combination. However, in subsequent cycles, the degradation rate decreases noticeably, especially after each 180-min interval suggesting partial deactivation of the catalyst over time. The degradation efficiency remains high throughout the cycles but exhibits a slight decline with each subsequent cycle. In the first cycle, degradation reaches 99.03% after 180 min, demonstrating strong catalytic performance. However, by the fourth cycle, efficiency slightly decreases to 96.62%. Additionally, Zaaboul *et. al*., [38] demonstrated that the P25 catalyst retains a substantial adsorption capacity for RB-203 dye after multiple photocatalysis cycles, although a reduction in efficiency is noted after multiple photocatalysis cycles, further emphasizing the importance of understanding catalyst behavior over repeated use in photocatalytic applications.

The decline in degradation efficiency of OTC using P25/500 after each cycle can be attributed to catalyst deactivation due to surface fouling, loss of active sites, and incomplete regeneration during the filtration, centrifugation, and drying steps between cycles. Despite these limitations, the catalyst maintains a reasonable degree of activity, as evidenced by $\ln(C_0/C_t)$ values exceeding 3.5 by the end of each cycle. The plateau in degradation efficiency during the later stages of each cycle suggests that the reaction reaches equilibrium after prolonged exposure, limiting further OTC breakdown. This trend points to the role of PDS may decline over time, requiring re-dosing to maintain consistent radical generation.

3.5 *Degradation of OTC and identification of intermediates via UPLC-MS/MS analysis*

In this study, OTC was rapidly degraded within the first 5 min and almost disappeared by the 90-min mark. The MS spectra of OTC degradation products are exhibited in Figure 19. The degradation of OTC in the 2L model suspension showed a significant decline in the OTC peak intensity, with some peaks completely disappearing as reaction time increased. This suggests the rapid breakdown of OTC over time. Notably, an anionic fragment with a mass-to-charge (m/z) ratio of 163 emerged as a prominent intermediate product, detected at relatively high levels at the 5-min (Figure 19(b)), 30-min (Figure 19(c)), and 90-min marks (Figure 19(d)). The blank sample, which contained only OTC at the beginning of the experiment, showed dominant ionic fragments with m/z values of 460 and 461—two forms of OTC—indicating that no degradation products were present in the initial state (Figure 19(a)).

The OTC peak sharply decreased or disappeared with the increase in the reaction time in 2L model suspension, and an anion with m/z of 163 was observed at a relatively high level at 5- (Figure 19(b)), 30- (Figure 19(c)), and 90-min marks (Figure 19(d)), which may be the main intermediate product. While dominant ionic fragments of OTC were m/z of 460 and 461 (two forms of OTC) in blank indicating that there is not any degradation product in these systems (Figure 19(a)).

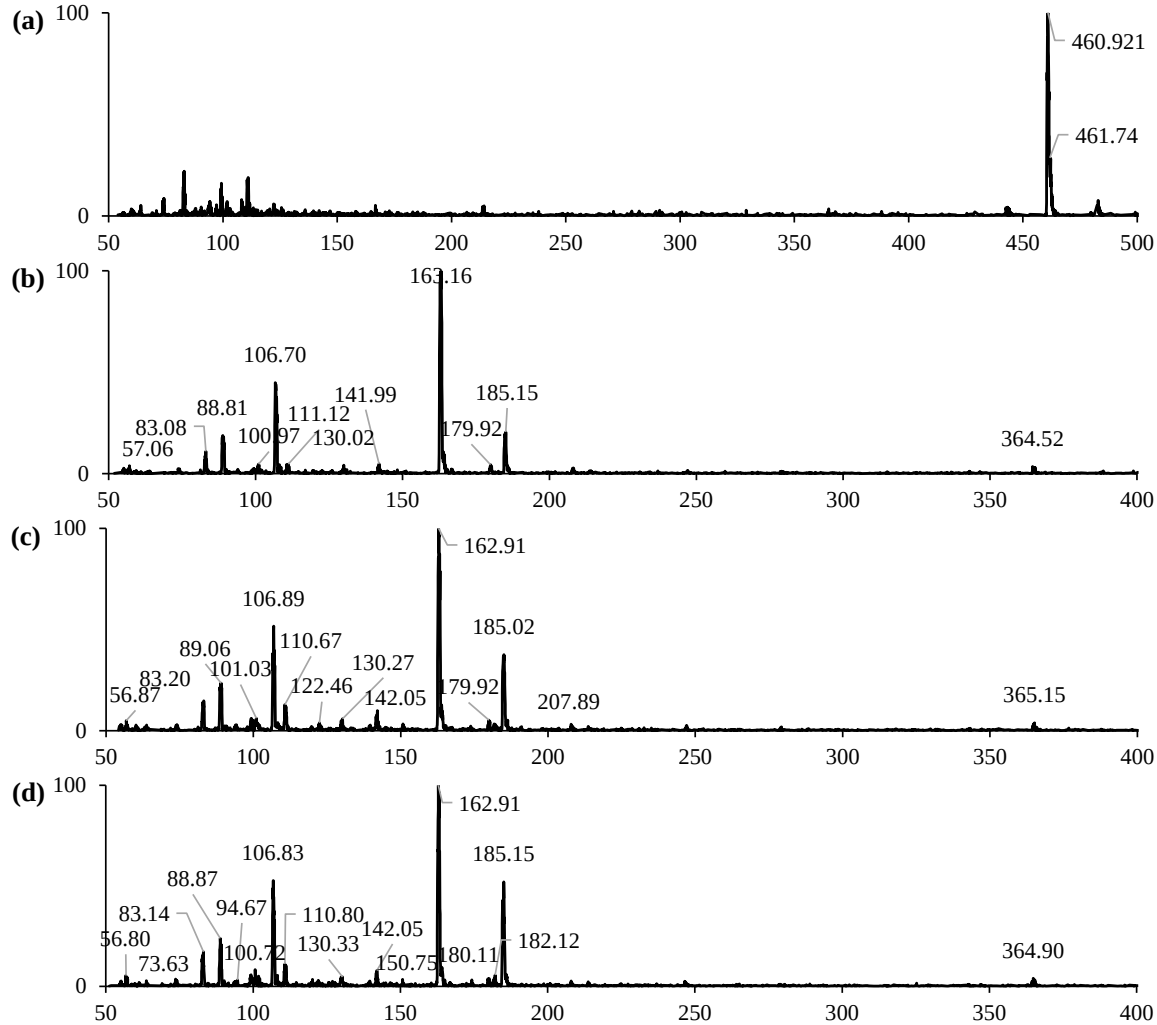

Figure 19: UPLC-MS/MS spectra of OTC at different degradation times: (a) blank, (b) 5 min, (c) 30 min, and (d) 90 min.

Based on the MS spectra shown in Figure 19, Figure 20 illustrates the proposed pathways by which OTC degrades into various intermediates. These pathways highlight how the major intermediates undergo transformations such as hydroxylation, hydrogenation, ring cleavage, ring-opening, demethylation, and dehydroxylation, ultimately leading to the formation of smaller organic molecules as degradation progresses.

In the first pathway, OTC is initially converted into the intermediate O1 (m/z = 342) through the loss of an amide group, a hydroxyl group, and the conversion of dimethylamine to amine on the carbon ring. This intermediate undergoes further transformations, including dehydroxylation, ring-opening, reduction, and demethylation, ultimately forming O11 (m/z = 163), which is consistent with the findings of Xin *et al.*, [39]. In the second pathway, OTC transforms into O4 (m/z = 365) through a series of reactions such as hydrogenation, ring cleavage, hydroxylation, and side-chain modifications, reflecting the outcomes reported by Chen *et al*., [40]. The third pathway involves the formation of O7 (m/z = 279) via the loss of carbonyl, hydroxyl, methyl, and amino groups, in agreement with the results of *He et al*., [41]. O7 is then converted into O8 (m/z = 227) through additional dehydroxylation and demethylation steps. As degradation advances, the

intermediates undergo oxidation, producing smaller organic molecules with m/z values of 185, 179, 163, 148, and 84, which are formed through dissociation and ring-opening reactions, in accordance with previous studies [42]–[44].

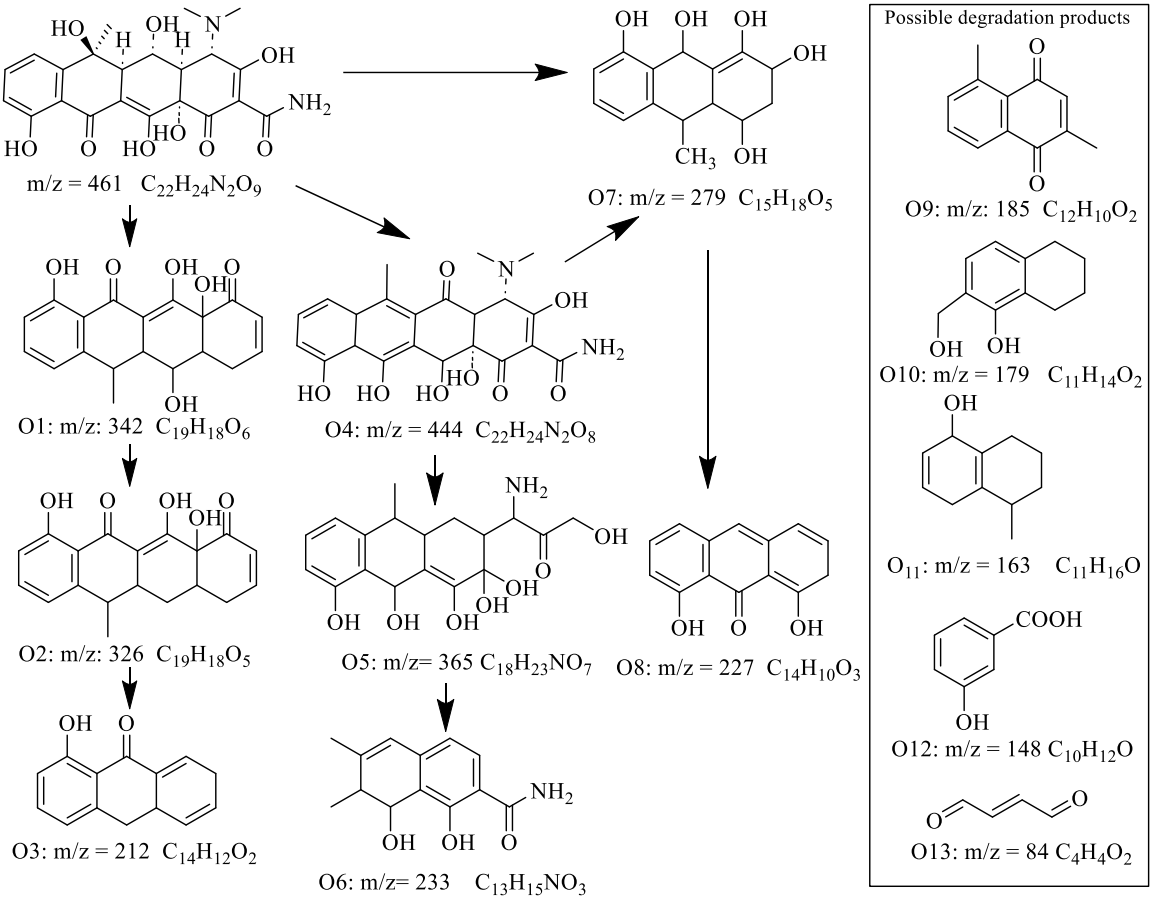

Figure 20: The proposed degradation by-product of OTC.

3.6 *Radical trapping tests*

Figure 21 shows the trends in OTC concentration over time under different radical scavengers: BQ, AO, NN, and MT. The analysis of these trends revealed their roles in photocatalytic degradation.

In this experiment, the mole-based analysis reveals the critical role of superoxide radicals in OTC degradation. With a TiO_2 concentration of 300 mg/L (3.76 mmol/L) and all scavengers at 5 mM (mole ratio of 1.33:1), BQ, a superoxide radical scavenger, completely inhibits degradation, reducing efficiency to 0% after 30 minutes. This indicates that superoxide radicals ($\bullet O_2^-$) are the dominant species in the photocatalytic degradation process, serving as crucial oxidizing agents that initiate and sustain the degradation reactions.

The role of different radicals in OTC degradation by P25 was investigated using various scavengers. The significant decrease in OTC degradation efficiency observed with BQ demonstrates its effect as a superoxide scavenger, resulting in a peak efficiency of only 1.79% after 15 min. This finding highlights the necessity of $\bullet O_2^-$ in the degradation pathway. In contrast, the effects of other scavengers underscored the involvement of additional radicals. AO resulted in a gradual decrease in OTC concentration, achieving an efficiency of 76.62% after 180 min. This observation supports the role of photogenerated holes (h^+) along with $\bullet O_2^-$ radicals in the degradation process, as holes

are known to directly oxidize organic pollutants, thereby enhancing the degradation efficiency.

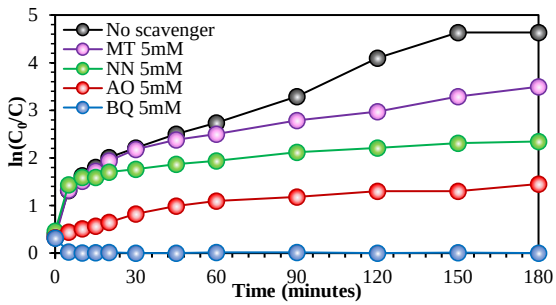

Figure 21: Performances of OTC photocatalysis degradation by using P25/500 catalyst and PDS with different quenchers under UV influence.

NN induced a notable reduction in OTC concentration, reaching an efficiency of 90.41% after 180 min. This further substantiates the role of $^1O_2$ in the degradation process, as NN selectively scavenges $^1O_2$, allowing for the continued oxidation of OTC through this pathway. The evidence suggests a synergistic action where both $\bullet O_2^-$ and $^1O_2$ actively participate in the mineralization of the antibiotic compound. MT led to a substantial decline in OTC concentration, with an efficiency of 96.97% after 180 min. This result indicates the involvement of hydroxyl radicals (•OH), which, although may contribute less significantly than superoxide radicals, enhance the overall oxidative capacity of the system by reacting with various organic compounds. Therefore, the order of radical contribution was found to be $^{\bullet}O_2^- > h^+ > {}^1O_2 > {}^{\bullet}OH$, emphasizing the predominant role of superoxide radicals in the process. Understanding these interactions not only elucidates the degradation mechanism but also aids in optimizing photocatalytic processes for effective antibiotic removal from wastewater. In comparison, Demyanenko *et. al.*, [45] revealed that singlet oxygen ($^1O_2$) adsorbed on the surface of TiO_2 exhibits a bathochromic spectral shift and shortened lifetime due to its interaction with TiO_2's polar surface groups, which influences its nonradiative relaxation and efficiency in photocatalytic processes.

3.7 *Mechanisms of OTC photocatalytic degradation using TiO_2 and PDS*

The photocatalytic degradation of OTC using TiO_2 with PDS involves a series of critical steps [46]. Initially, when TiO_2 (specifically P25/500) is exposed to UV light with energy exceeding its band gap (approximately 3.2 eV [47]), electron-hole pairs are generated as described by Equation (2).

$$TiO_2 + h\nu \rightarrow TiO_2\,(e^- + h^+) \quad (2)$$

These charge carriers are crucial for initiating photocatalytic reactions. The photo-generated electrons (e^-) and holes (h^+) then participate in redox reactions, leading to the formation of various ROSs such as superoxide radicals ($^{\bullet}O_2^-$), hydroxyl radicals ($^{\bullet}OH$), and hydrogen peroxide (H_2O_2), as shown in Equations (3) and (4) [48]. The formation of hydroxyl radicals can also occur through the reaction of holes with hydroxide ions (OH^-) (Equation 5) [49]. The electrons reduce oxygen to superoxide radicals, while the holes oxidize water to hydroxyl radicals.

$$e^- + O_2 \rightarrow {}^{\bullet}O_2^- \quad (3)$$

$$h^+ + H_2O \rightarrow {}^{\bullet}OH + H^+ \quad (4)$$

$$h^+ + OH^- \rightarrow {}^{\bullet}OH \quad (5)$$

Additionally, superoxide radicals further react with protons to form hydrogen peroxide (H_2O_2) (Equation 6).

$$2{}^{\bullet}O_2^- + 2H^+ \rightarrow H_2O_2 + O_2 \quad (6)$$

Under UV light, H_2O_2 decomposes to produce additional hydroxyl radicals (Equation 7) [50]. This chain of reactions significantly enhances the oxidative capacity of the system, contributing to the efficient degradation of OTC.

$$H_2O_2 + h\nu \rightarrow 2{}^{\bullet}OH \quad (7)$$

The introduction of PDS into the system provides an additional pathway for radical formation. PDS reacts with electrons to produce sulfate radicals ($SO_4^{\bullet-}$) (Equation 8) [51]. These sulfate radicals can further react with water to produce hydroxyl radicals ($^{\bullet}OH$) and other species, as shown in Equation (13). Hydroxyl radicals can then interact with molecular oxygen to form superoxide radicals ($^{\bullet}O_2^-$) and hydrogen peroxide (H_2O_2), as indicated by Equations (10) and (15) [46], [52], [53]. Additionally, sulfate radicals can react with hydroxide ions to generate more hydroxyl radicals (Equation (14)), thus amplifying the oxidative capacity. However, it has

been reported that in real wastewater treatment scenarios, excess PDS can lead to scavenging effects. Surplus PDS results in the formation of weaker oxidants such as sulfate radicals and hydroperoxide radicals (HO_2^-), rather than more potent oxidants [54], as reflected in Equations (9) and (12) [55]. This shift in the oxidative profile can impact the efficiency of contaminant degradation. The reaction in Equation (11) produces the hydrogen sulfate radical ($HSO_4^{\bullet}$), which persists relatively well in mildly acidic conditions and may contribute to selective oxidation or participate in scavenging effect. The array of reactive oxygen species, including hydroxyl radicals, superoxide radicals, sulfate radicals, and singlet oxygen ($^1O_2$), then actively engages with contaminants like OTC, leading to their degradation.

$$S_2O_8^{2-} + e^- \rightarrow SO_4^{\bullet-} + SO_4^{2-} \quad (8)$$

$$S_2O_8^{2-} + 2H_2O \rightarrow HO_2^- + 2\,SO_4^{2-} + 3H^+ \quad (9)$$

$$HO_2^- + S_2O_8^{2-} \rightarrow SO_4^{\bullet-} + SO_4^{2-} + H^+ + {}^{\bullet}O_2^- \quad (10)$$

$$SO_4^{\bullet-} + H^+ \rightarrow HSO_4^{\bullet} \quad (11)$$

$$4SO_4^{\bullet-} + 2H_2O \rightarrow 4HSO_4^- + {}^1O_2 \quad (12)$$

$$SO_4^{\bullet-} + H_2O \rightarrow SO_4^{2-} + {}^{\bullet}OH + OH^- \quad (13)$$

$$SO_4^{\bullet-} + OH^- \rightarrow {}^{\bullet}OH + SO_4^{2-} \quad (14)$$

$${}^{\bullet}OH + {}^{\bullet}OH \rightarrow H_2O_2 \quad (15)$$

The ROS, including hydroxyl radicals, superoxide radicals, sulfate radicals, and singlet oxygen, then react with OTC, leading to its degradation. This interaction can be summarized by the reaction:

$$[{}^{\bullet}O_2^-, {}^1O_2, {}^{\bullet}OH, h^+] + OTC \rightarrow \text{degraded products} \quad (16)$$

Figure 22 illustrates the detailed mechanism of ROS generation and their roles in the photocatalytic degradation of OTC, highlighting the interconnected processes and pathways involved.

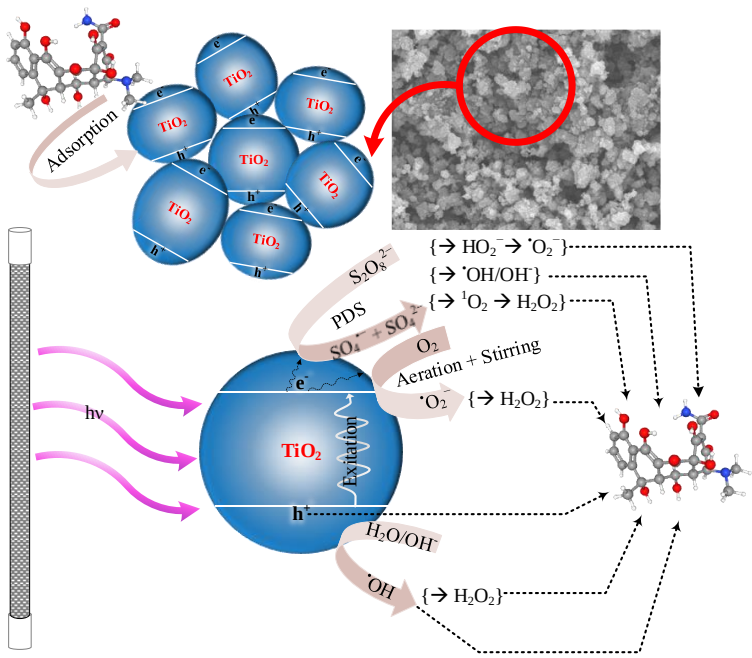

Figure 22: Mechanism of ROS generation and degradation pathways for OTC in the TiO_2/PDS system.

4 Conclusions

This research provides valuable insights into the potential application of TiO_2 photocatalysis for the removal of OTC, which involved synthesizing P25 TiO_2, evaluating the photocatalytic degradation of 10 ppm OTC with PDS at 500 ppm and UV irradiation, conducting radical trapping tests to identify key radicals like ${}^{\bullet}O_2^-$, analyzing energy consumption with an UV lamp and air pump, performing LC-MS to track

OTC concentration changes and identify intermediates, and comparing photocatalytic efficiency against control tests with no catalyst. At an initial concentration of 10 ppm, synthesized P25 achieved a remarkable degradation efficiency of 96.62% after 180 minutes with PDS at 100 ppm. This performance stands in stark contrast to the no-catalyst control, which only attained 31.79% degradation. Results indicated that a slightly acidic to neutral pH range and a PDS concentration of 500 ppm were optimal for efficient OTC removal. Despite challenges in real-world applications due to complex water matrices, findings suggest that additional treatment steps can further enhance efficacy. The energy consumption of 42 Wh over 180 min demonstrated a feasible approach for industrial-scale applications. Additionally, LC-MS analysis confirmed significant reductions in OTC concentration, with key intermediate products identified. Moreover, the investigation utilized scavengers to identify the role of radicals in the photocatalytic degradation of OTC. The results emphasized the significant contribution of $^{\bullet}O_2^-$ radicals to the process, reinforcing the effectiveness of TiO_2 photocatalysis. Future work should focus on optimizing photocatalyst formulations and operational parameters to further enhance scalability and efficiency.

Acknowledgments

This research is funded by Vietnam National University Ho Chi Minh City (VNU-HCM) under grant number: B2023-20-20.

Author Contributions

T.Q.T.: conceptualization, validation, visualization, writing an original draft, N.T.T.H.: investigation; P.T.T: methodology, supervision; N.T.T.: formal analysis, data curation; P.T.L.: data curation, funding acquisition, N.T.T.: visualization, reviewing and editing, P.P.T.: research design, investigation; L.T.T.: software, investigation, N.N.H.: reviewing and editing, resources, funding acquisition, supervision, project administration. All authors have read and agreed to the published version of the manuscript.

Conflicts of Interest

The authors declare no conflict of interest.

References

[1] P. Huo, X. Gao, Z. Lu, X. Liu, Y. Luo, W. Xing, J. Li, and Y. Yan, "Photocatalytic degradation of antibiotics in water using metal ion@ TiO2/HNTs under visible light," *Desalination and Water Treatment*, vol. 52, pp. 6985–6995, 2014.

[2] P. T. P. Hoa, S. Managaki, N. Nakada, H. Takada, A. Shimizu, D. H. Anh, P. H. Viet, and S. Suzuki, "Antibiotic contamination and occurrence of antibiotic-resistant bacteria in aquatic environments of northern Vietnam," *Science of the Total Environment*, vol. 409, pp. 2894–2901, 2011.

[3] M. Teuber, "Veterinary use and antibiotic resistance," *Current opinion in microbiology*, vol. 4, pp. 493–499, 2001.

[4] D. A. Goff, R. Kullar, E. J. Goldstein, M. Gilchrist, D. Nathwani, A. C. Cheng, K. A. Cairns, K. EscandÃ³n-Vargas, M. V. Villegas, and A. Brink, "A global call from five countries to collaborate in antibiotic stewardship: united we succeed, divided we might fail," *The Lancet Infectious Diseases*, vol. 17, pp. e56–e63, 2017.

[5] E. Y. Klein, M. Milkowska-Shibata, K. K. Tseng, M. Sharland, S. Gandra, C. Pulcini, and R. Laxminarayan, "Assessment of WHO antibiotic consumption and access targets in 76 countries, 2000–15: An analysis of pharmaceutical sales data," *The Lancet Infectious Diseases*, vol. 21, pp. 107–115, 2021.

[6] A. J. Browne, M. G. Chipeta, G. Haines-Woodhouse, E. P. Kumaran, B. H. K. Hamadani, S. Zaraa, N. J. Henry, A. Deshpande, R. C. Reiner, and N. P. Day, "Global antibiotic consumption and usage in humans, 2000–18: A spatial modelling study," *The Lancet Planetary Health*, vol. 5, pp. e893–e904, 2021.

[7] P. K. Thai, L. X. Ky, V. N. Binh, P. H. Nhung, P. T. Nhan, N. Q. Hieu, N. T. T. Dang, N. K. B. Tam, and N. T. K. Anh, "Occurrence of antibiotic residues and antibiotic-resistant bacteria in effluents of pharmaceutical manufacturers and other sources around Hanoi, Vietnam," *Science of The Total Environment*, vol. 645, pp. 393–400, 2018.

[8] Y. Ben, C. Fu, M. Hu, L. Liu, M. H. Wong, and C. Zheng, "Human health risk assessment of antibiotic resistance associated with antibiotic residues in the environment: A review,"

Environmental Research, vol. 169, pp. 483–493, 2019.

[9] J. L. Martinez, "Environmental pollution by antibiotics and by antibiotic resistance determinants," *Environmental Pollution*, vol. 157, pp. 2893–2902, 2009.

[10] Z.-j. LI, W.-n. QI, F. Yao, Y.-w. LIU, S. Ebrahim, and L. Jian, "Degradation mechanisms of oxytetracycline in the environment," *Journal of Integrative Agriculture*, vol. 18, pp. 1953–1960, 2019.

[11] M. L. Tran, S.-W. Deng, C.-C. Fu, and R.-S. Juang, "Efficient removal of antibiotic oxytetracycline from water using optimized montmorillonite-supported zero-valent iron nanocomposites," *Environmental Science and Pollution Research*, vol. 27, pp. 30853–30867, 2020.

[12] L. Q. Huong, T. T. T. Hang, P. T. Ngoc, C. V. Tuat, V. I. Erickson, and P. Padungtod, "Pilot monitoring of antimicrobial residues in chicken and pork in Vietnam," *Journal of Food Protection*, vol. 83, pp. 1701–1706, 2020.

[13] D. S. Shen, X. Q. Tao, J. L. Shentu, and M. Z. Wang, "Residues of veterinary antibiotics in pig feeds and manures in Zhejiang Province," *Advanced Materials Research*, vol. 1010, pp. 301–304, 2014.

[14] M. D. Hernando, M. Mezcua, A. R. Fernández-Alba, and D. Barceló, "Environmental risk assessment of pharmaceutical residues in wastewater effluents, surface waters and sediments," *Talanta*, vol. 69, pp. 334–342, 2006.

[15] N. Olama, M. Dehghani, and M. Malakootian, "The removal of amoxicillin from aquatic solutions using the TiO 2/UV-C nanophotocatalytic method doped with trivalent iron," *Applied Water Science*, vol. 8, pp. 1–12, 2018.

[16] W. Wang, X. Liu, J. Fang, and C. Lu, "TiO_2@ g-C_3N_4 heterojunction with directional charge migration behavior for photodegradation of tetracycline antibiotics," *Materials Letters*, vol. 236, pp. 622–624, 2019.

[17] A. Fujishima and X. Zhang, "Titanium dioxide photocatalysis: Present situation and future approaches," *Comptes Rendus Chimie*, vol. 9, pp. 750–760, 2006.

[18] M. Farzadkia, E. Bazrafshan, A. Esrafili, J.-K. Yang, and M. Shirzad-Siboni, "Photocatalytic degradation of Metronidazole with illuminated TiO_2 nanoparticles," *Journal of Environmental Health Science and Engineering*, vol. 13, pp. 1–8, 2015.

[19] N. T. C. Tien, T. T. B. Huyen, N. T. Thuy, D. Van Thanh, N. T. Thanh, and N. N. Huy, "Degradation of enrofloxacin by photocatalysis using titanium dioxide nanomaterials," in *IOP Conference Series: Earth and Environmental Science*, 2021, Art. no. 012033.

[20] B. Kakavandi, N. Bahari, R. R. Kalantary, and E. D. Fard, "Enhanced sono-photocatalysis of tetracycline antibiotic using TiO_2 decorated on magnetic activated carbon (MAC@ T) coupled with US and UV: A new hybrid system," *Ultrasonics Sonochemistry*, vol. 55, pp. 75–85, 2019.

[21] Q. Cai and J. Hu, "Effect of UVA/LED/TiO_2 photocatalysis treated sulfamethoxazole and trimethoprim containing wastewater on antibiotic resistance development in sequencing batch reactors," *Water Research*, vol. 140, pp. 251–260, 2018.

[22] A. Mekkaoui, E. G. Temam, S. Rahmane, and B. Gasmi, "A new study on the effect of pure anatase TiO_2 film thickness on gentian violet photodegradation under sunlight: Considering the effect of hole scavengers," *Trends in Sciences*, vol. 20, p. 3766, 2023.

[23] M. Althamthami, E. Guettaf Temam, H. B. Temam, R. Saad, and G. G. Hasan, "Improved photocatalytic activity under the sunlight of high transparent hydrophilic Bi-doped TiO_2 thin-films," *Journal of Photochemistry and Photobiology A: Chemistry*, vol. 443, 2023, Art. no. 114818.

[24] E. Guettaf Temam, F. Djani, S. Rahmane, H. Ben Temam, and B. Gasmi, "Photocatalytic activity of Al/Ni doped TiO_2 films synthesized by sol-gel method: Dependence on thickness and crystal growth of photocatalysts," *Surfaces and Interfaces*, vol. 31, 2022, Art. no. 102077.

[25] C. Sriwong, K. Choojun, and S. Sriwong, "High photocatalytic performance of 3D porous-structured TiO_2@ natural rubber hybrid sheet on the removal of indigo carmine dye in water," *SN Applied Sciences*, vol. 1, p. 864, 2019.

[26] H. Znad and Y. Kawase, "Synthesis and characterization of S-doped Degussa P25 with application in decolorization of Orange II dye as a model substrate," *Journal of Molecular Catalysis A: Chemical*, vol. 314, pp. 55–62, 2009.

[27] J. C. Yu, J. Yu, W. Ho, Jiang, and Zhang, "Effects of F-doping on the photocatalytic activity and microstructures of nanocrystalline TiO2 powders," *Chemistry of Materials*, vol. 14, pp. 3808–3816, 2002.

[28] F. Scarpelli, T. F. Mastropietro, T. Poerio, and N. Godbert, "Mesoporous TiO_2 thin films: State of the art," *Titanium Dioxide-Material for a Sustainable Environment*, vol. 508, pp. 135–142, 2018.

[29] M. Takeuchi, G. Martra, S. Coluccia, and M. Anpo, "Investigations of the structure of H2O clusters adsorbed on TiO_2 surfaces by near-infrared absorption spectroscopy," *The Journal of Physical Chemistry B*, vol. 109, pp. 7387–7391, 2005.

[30] E. Felis, M. Buta-Hubeny, W. Zieliński, J. Hubeny, M. Harnisz, S. Bajkacz, and E. Korzeniewska, "Solar-light driven photodegradation of antimicrobials, their transformation by-products and antibiotic resistance determinants in treated wastewater," *Science of The Total Environment*, vol. 836, 2022, Art. no. 155447.

[31] X. Jin, H. Xu, S. Qiu, M. Jia, F. Wang, A. Zhang, and X. Jiang, "Direct photolysis of oxytetracycline: Influence of initial concentration, pH and temperature," *Journal of Photochemistry and Photobiology A: Chemistry*, vol. 332, pp. 224–231, 2017.

[32] G. Dong, B. Chen, B. Liu, L. J. Hounjet, Y. Cao, S. R. Stoyanov, M. Yang, and B. Zhang, "Advanced oxidation processes in microreactors for water and wastewater treatment: Development, challenges, and opportunities," *Water Research*, vol. 211, 2022, Art. no. 118047.

[33] M. Sharma, A. Yadav, M. Mandal, and K. Dubey, "TiO_2 based photocatalysis: A valuable approach for the removal of pharmaceuticals from aquatic environment," *International Journal of Environmental Science and Technology*, vol. 20, pp. 4569–4584, 2023.

[34] R. Sabouni and H. Gomaa, "Comparative analysis of aeration and oscillation in a suspended catalyst photocatalytic membrane reactor," *Chemical Engineering Research and Design*, vol. 173, pp. 55–62, 2021.

[35] E. Azadi, A. Akbar Zinatizadeh, D. Yazdani, M. Sillanpää, and M. Joshaghani, "The photodegradation of oxytetracycline by Degussa P25-TiO_2/FeO/ZnO ternary chain heterojunction in the presence of persulfate under visible light irradiation: The optimization and kinetic study," *Inorganic Chemistry Communications*, vol. 166, 2024, Art. no. 112600.

[36] Y. Zhang, Q. Chen, H. Qin, J. Huang, and Y. Yu, "Identification of reactive oxygen species and mechanism on visible light-induced photosensitized degradation of oxytetracycline," *International Journal of Environmental Research and Public Health*, vol. 19, no. 23, 2022, Art. no. 15550.

[37] S. Giannakis, K.-Y. A. Lin, and F. Ghanbari, "A review of the recent advances on the treatment of industrial wastewaters by Sulfate Radical-based Advanced Oxidation Processes (SR-AOPs)," *Chemical Engineering Journal*, vol. 406, 2021, Art. no. 127083.

[38] F. Zaaboul, C. Haoufazane, A. Kari, R. Salim, K. Azzaoui, R. Sabbahi, and A. El Hourch, "Study of Reactive blue 203 removal by TiO_2-P25 adsorption combined with photocatalysis for its degradation," *Moroccan Journal of Chemistry*, vol. 12, pp. 1664–1682, 2024.

[39] Y. Xin, P. Zhang, J. Shen, and S. Ren, "Development of vitamin B6-mediated biochar with nano zero-valent iron coating for oxytetracycline removal through adsorption and degradation under harsh acidic conditions," *Water*, vol. 14, no. 17, p. 2734, 2022.

[40] Y. Chen, K. Zhu, W. Qin, Z. Jiang, Z. Hu, M. Sillanpää, and K. Yan, "Enhanced electron transfer using $NiCo_2O_4$@ C hollow nanocages with an electron-shuttle effect for efficient tetracycline degradation," *Chemical Engineering Journal*, vol. 488, 2024, Art. no. 150786.

[41] L. He, H. Li, J. Wang, Q. Gao, and X. Li, "Peroxymonosulfate activation by Co-doped magnetic Mn_3O_4 for degradation of oxytetracycline in water," *Environmental Science and Pollution Research*, vol. 29, pp. 39249–39265, 2022.

[42] J. Xu, H. Zhang, J. Ma, L. Zhou, Q. Zhao, and Z. Ye, "A polystyrene resin in situ supported PANI/Fe_3O_4 composite as a heterogeneous Fenton catalyst for the efficient degradation of tetracycline in water," *Journal of Materials Chemistry A*, vol. 12, pp. 22180–22200, 2024.

[43] P. T. Le, T. P. Nguyen, T. H. Do, H. N. Nguyen, T. M. T. Dinh, T. T. Phan, T. Tsubota, and T. D. Nguyen, "Synergistic effect of the heterojunction gC_3N_4/Bi_2MoO_6/clinoptilolite to enhance the photocatalytic degradation of antibiotics in water in the presence of persulfate," *Environmental*

Science: Water Research & Technology, vol. 10, pp. 2665–2687, 2024.

[44] Z. S. Wei, X. L. Chen, Z. S. Huang, H. Y. Jiao, and X. L. Xiao, "Insights into the removal of gaseous oxytetracycline by combined ozone and membrane biofilm reactor," *Environmental Engineering Research*, vol. 27, pp. 210469–210470, 2021.

[45] A. V. Demyanenko, A. S. Bogomolov, N. V. Dozmorov, A. I. Svyatova, A. P. Pyryaeva, V. G. Goldort, S. A. Kochubei, and A. V. Baklanov, "Singlet oxygen $^1O_2$ in photocatalysis on TiO_2. Where does it come from?," *The Journal of Physical Chemistry C*, vol. 123, pp. 2175–2181, 2019.

[46] N. T. Dung, P. T. H. Hanh, V. D. Thao, N. T. Thuy, D. T. M. Thanh, N. T. Phuong, K.-Y. A. Lin, and N. N. Huy, "Decomposition and mineralization of glyphosate herbicide in water by radical and non-radical pathways through peroxymonosulfate activation using Co_3O_4/gC_3N_4: A comprehensive study," *Environmental Science: Water Research & Technology*, vol. 9, pp. 221–234, 2023.

[47] I. Arora, H. Chawla, A. Chandra, S. Sagadevan, and S. Garg, "Advances in the strategies for enhancing the photocatalytic activity of TiO_2: Conversion from UV-light active to visible-light active photocatalyst," *Inorganic Chemistry Communications*, vol. 143, 2022, Art. no. 109700.

[48] S. P. Mulakov, P. M. Gotovtsev, A. A. Gainanova, G. V. Kravchenko, G. M. Kuz'micheva, and V. V. Podbel'skii, "Generation of the Reactive Oxygen Species on the surface of nanosized titanium (IV) oxides particles under UV-irradiation and their connection with photocatalytic properties," *Journal of Photochemistry and Photobiology A: Chemistry*, vol. 393, 2020, Art. no. 112424.

[49] M. G. Kim, J. M. Kang, J. E. Lee, K. S. Kim, K. H. Kim, M. Cho, and S. G. Lee, "Effects of calcination temperature on the phase composition, photocatalytic degradation, and virucidal activities of TiO_2 nanoparticles," *ACS Omega*, vol. 6, pp. 10668–10678, 2021.

[50] N. Mediouni, F. Dappozze, L. Khrouz, S. Parola, A. B. H. Amara, H. B. Rhaiem, N. Jaffrezic-Renault, P. Namour, and C. Guillard, "Correlation between Photocatalytic Properties of ZnO and Generation of Hydrogen Peroxide—Impact of Composite ZnO/TiO_2 Rutile and Anatase," *Catalysts*, vol. 12, p. 1445, 2022.

[51] M. Ge, Z. Hu, J. Wei, Q. He, and Z. He, "Recent advances in persulfate-assisted TiO_2-based photocatalysis for wastewater treatment: Performances, mechanism and perspectives," *Journal of Alloys and Compounds*, vol. 888, 2021, Art. no. 161625.

[52] A. A. Babaei, M. Golshan, and B. Kakavandi, "A heterogeneous photocatalytic sulfate radical-based oxidation process for efficient degradation of 4-chlorophenol using TiO_2 anchored on Fe oxides@ carbon," *Process Safety and Environmental Protection*, vol. 149, pp. 35–47, 2021.

[53] G. Zhang, L. Zhao, X. Hu, X. Zhu, and F. Yang, "Synergistic activation of sulfate by TiO_2 nanotube arrays-based electrodes for berberine degradation: Insight into pH-dependant ORR-strengthened reactive radicals co-generation mechanism," *Applied Catalysis B: Environmental*, vol. 313, 2022, Art. no. 121453.

[54] W.-J. Xue, Y.-H. Cui, Z.-Q. Liu, S.-Q. Yang, J.-Y. Li, and X.-L. Guo, "Treatment of landfill leachate nanofiltration concentrate after ultrafiltration by electrochemically assisted heat activation of peroxydisulfate," *Separation and Purification Technology*, vol. 231, 2020, Art. no. 115928.

[55] J. Wang and S. Wang, "Reactive species in advanced oxidation processes: Formation, identification and reaction mechanism," *Chemical Engineering Journal*, vol. 401, 2020, Art. no. 126158.